



Kent Academic Repository

Skinner, Benjamin M., Bacon, Joanne, Rathje, Claudia C., Larson, Erica L., Kopania, Emily E. K., Good, Jeffrey M., Affara, Nabeel A. and Ellis, Peter J.I. (2019) *Automated nuclear cartography reveals conserved sperm chromosome territory localization across 2 million years of mouse evolution*. *Genes*, 10 (2).

Downloaded from

<https://kar.kent.ac.uk/72162/> The University of Kent's Academic Repository KAR

The version of record is available from

<https://doi.org/10.3390/genes10020109>

This document version

Author's Accepted Manuscript

DOI for this version

Licence for this version

UNSPECIFIED

Additional information

Versions of research works

Versions of Record

If this version is the version of record, it is the same as the published version available on the publisher's web site. Cite as the published version.

Author Accepted Manuscripts

If this document is identified as the Author Accepted Manuscript it is the version after peer review but before type setting, copy editing or publisher branding. Cite as Surname, Initial. (Year) 'Title of article'. To be published in **Title of Journal**, Volume and issue numbers [peer-reviewed accepted version]. Available at: DOI or URL (Accessed: date).

Enquiries

If you have questions about this document contact ResearchSupport@kent.ac.uk. Please include the URL of the record in KAR. If you believe that your, or a third party's rights have been compromised through this document please see our [Take Down policy](https://www.kent.ac.uk/guides/kar-the-kent-academic-repository#policies) (available from <https://www.kent.ac.uk/guides/kar-the-kent-academic-repository#policies>).

Automated nuclear cartography reveals conserved sperm chromosome territory localization across 2 million years of mouse evolution

Benjamin Matthew Skinner^{1*}, Joanne Bacon¹, Claudia Cattoni Rathje², Erica Lee Larson^{3,4}, Emily Emiko Konishi Kopania⁴, Jeffrey Martin Good⁴, Nabeel Ahmed Affara¹ and Peter James Ivor Ellis^{2*}

¹ Department of Pathology, University of Cambridge, Cambridge, CB2 1QP, UK; bms41@cam.ac.uk (B.M.S); jb552@cam.ac.uk (J.B.); na106@cam.ac.uk (N.A.)

² School of Biosciences, University of Kent, Canterbury, CT2 7NJ, UK; C.C.Rathje@kent.ac.uk (C.C.R); P.J.I.Ellis@kent.ac.uk (P.J.I.E)

³ Department of Biological Sciences, University of Denver, Denver, CO, USA; erica.larson@du.edu

⁴ Division of Biological Sciences, University of Montana, MT, USA; emily.kopania@umconnect.umt.edu (E.E.K.K); jeffrey.good@mso.umt.edu (J.M.G)

* Correspondence: bms41@cam.ac.uk

Received: date; Accepted: date; Published: date

Abstract: Measurements of nuclear organization in asymmetric nuclei in 2D images have traditionally been manual. This is exemplified by attempts to measure chromosome position in sperm samples, typically by dividing the nucleus into zones, and manually scoring which zone a FISH signal lies in. This is time consuming, limiting the number of nuclei that can be analyzed, and prone to subjectivity. We have developed a new approach for automated mapping of FISH signals in asymmetric nuclei, integrated into an existing image analysis tool for nuclear morphology. Automatic landmark detection defines equivalent structural regions in each nucleus, then dynamic warping of the FISH images to a common shape allows us to generate a composite of the signal within the entire cell population. Using this approach, we mapped the positions of the sex chromosomes and two autosomes in three mouse lineages (*Mus musculus domesticus*, *Mus musculus musculus* and *Mus spretus*). We found that in all three, chromosomes 11 and 19 tend to interact with each other, but are shielded from interactions with the sex chromosomes. This organization is conserved across 2 million years of mouse evolution.

Keywords: nuclear organization; sperm; morphometrics; chromosome painting

1. Introduction

Studies of the sub-nuclear localisation of chromatin often use fluorescence in-situ hybridisation to detect DNA or RNA, or immunostaining to detect proteins. The images are subsequently analysed either manually, or using some automated analysis tool. If the nucleus is circular or elliptical, it is commonly divided into concentric shells of equal area and the proportion of signal in each shell is measured (e.g. [1–3]). This has been amenable to automation, allowing analysis of thousands of cells, which, with appropriate statistical treatment, can yield valuable data at a scale that is still beyond the scope of 3D imaging techniques in time and cost.

However, if the nucleus is asymmetric, such as in sperm, a shell analysis is not sufficient. Frequently, nuclei are manually divided into geometric regions, and the number of nuclei with signals in each region are counted. For example, in spatulate sperm such as pig or human, positions of loci are located into anterior, medial and posterior regions [4–6], or measured by proportional position along each axis [7]. Rodent sperm have a more interesting, falciform, hooked shape: they have two axes of asymmetry, the anterior-posterior and the dorsal-ventral axis. This means that the location of a FISH signal can - in principle - be unambiguously localised and compared between nuclei. The determination of chromosome position is still manual, with more regions of the nucleus

47 into which a signal may be assigned [8,9], or described without quantitation [10]. This is both
48 time-consuming, and subjective, limiting the numbers of nuclei that can be analysed.

49 The positions of chromosomes or other loci in gametes (particularly sperm) is of great interest
50 due to both the association of nuclear organisation with fertility in the clinic, in agriculture, and in
51 evolutionary biology. Chromosome position has been linked with infertility in human males; men
52 presenting with fertility problems have less consistent chromosome territories than healthy men
53 [11–13]. Similarly, in farm animals, studies of nuclear organisation have discovered conserved sperm
54 chromosome territories in boars [4], and wider evolutionary studies have shown conservation of
55 some chromosomes - such as the X - from eutherian mammals to marsupial mammals and
56 monotremes [14].

57 Newer sequencing-based approaches, such as Hi-C are being used to produce 3D maps of
58 chromatin structure across multiple - and even single - nuclei [15–17]. Validating these results by
59 microscopy is harder due to the number of cells that must be analysed, yet is necessary for our
60 understanding of how chromatin patterns seen across millions of cells relate to chromatin structure
61 within an individual nucleus. Three-dimensional imaging such as confocal microscopy provides
62 high quality position information, but is time-consuming and costly in comparison to 2D
63 fluorescence imaging.

64 Given this, there is a need to quickly and robustly assay nuclear organisation in 2D fluorescence
65 microscopy images with greater precision than is currently available. Here, we demonstrate the use
66 of automatic landmark detection in nuclei to rapidly localise, aggregate and compare nuclear signals
67 without need for precise detection of the signal boundaries, or extensive manual thresholding and
68 curation. We use this method to investigate the conservation of nuclear organisation between three
69 mouse lineages, *Mus musculus musculus*, *Mus musculus domesticus* and *Mus spretus*. Of these, *M.*
70 *spretus* has a notably different nuclear shape [18] to the others, being shorter and wider, allowing us
71 to test whether chromosome position is conserved across structurally equivalent regions.

72 2. Materials and Methods

73 2.1 Sample collection

74
75 We collected sperm from wild-derived inbred mouse strains *Mus musculus musculus* (PWK/PhJ),
76 *M. m. domesticus* (LEWES/EiJ) and *Mus spretus* (STF). All animal procedures were subject to local
77 ethical review by the University of Montana Institute for Animal Care and Use Committee (protocol
78 identification number 002-13JGDBS-011613, approved January 16, 2013). Animals were bred at the
79 University of Montana from mice purchased from Jackson Laboratories (Bar Harbor, ME) or were
80 acquired from Francois Bonhomme (University of Montpellier). Animals were housed singly or in
81 small groups, sacrificed via CO₂ followed by cervical dislocation, and tissues were collected *post*
82 *mortem* for analysis. Sperm were collected and fixed in 3:1 methanol-acetic acid as previously
83 described [18].

84 85 2.2 Fluorescence in-situ hybridisation (FISH)

86
87 Fixed sperm were dropped on poly-lysine slides, air-dried, and aged at 70°C for one hour. Sperm
88 were swelled in 10mM DTT in 0.1M Tris-Hcl for 30 minutes at room temperature (RT). Slides were
89 rinsed in 2xSSC (saline sodium citrate) and dehydrated through an ethanol series (70%, 80%, 100%,
90 2mins at RT). Chromatin was relaxed by incubating slides in 0.1mg/ml pepsin in 0.01N HCl at 37°C for
91 20 mins. Nuclei were permeabilized in 0.5% IGEPAL CA-630, 0.5% Triton-X-100 at 4°C for 30 minutes,
92 and dehydrated through an ethanol series. Slides and chromosome paints for chrX, Y, 11 and 19
93 (Cytocell, AMP-0XG, AMP-0YR, AMP-11G, AMP-19R) were separately denatured in 70% formamide
94 at 75°C for 5 minutes, then slides were dehydrated through an ethanol series. Probes were
95 co-hybridised in pairs of 4µl each of: chrX and chrY; chrX and chr19; chr11 and chr19. The probes were
96 added to the slides, coverslips were sealed with rubber cement, and the slides were hybridised for 48
97 hours at 37°C. Coverslips were removed, and slides were washed in 0.7xSSC, 0.3% Tween-20 at 73°C

98 for 3 minutes to remove unbound probe, then washed in 2xSSC for 2 minutes at RT, rinsed in water
99 and air-dried in the dark. Slides were counterstained with 16µl VectorShield with DAPI (Vector Labs)
100 under a 22x50mm cover slip and imaged at 100x on an Olympus BX-61 epifluorescence microscope
101 equipped with a Hamamatsu Orca-ER C4742-80 cooled CCD camera and appropriate filters. Images
102 were captured using Smart-Capture 3 (Digital Scientific UK) with fixed exposure times for each
103 fluorochrome.

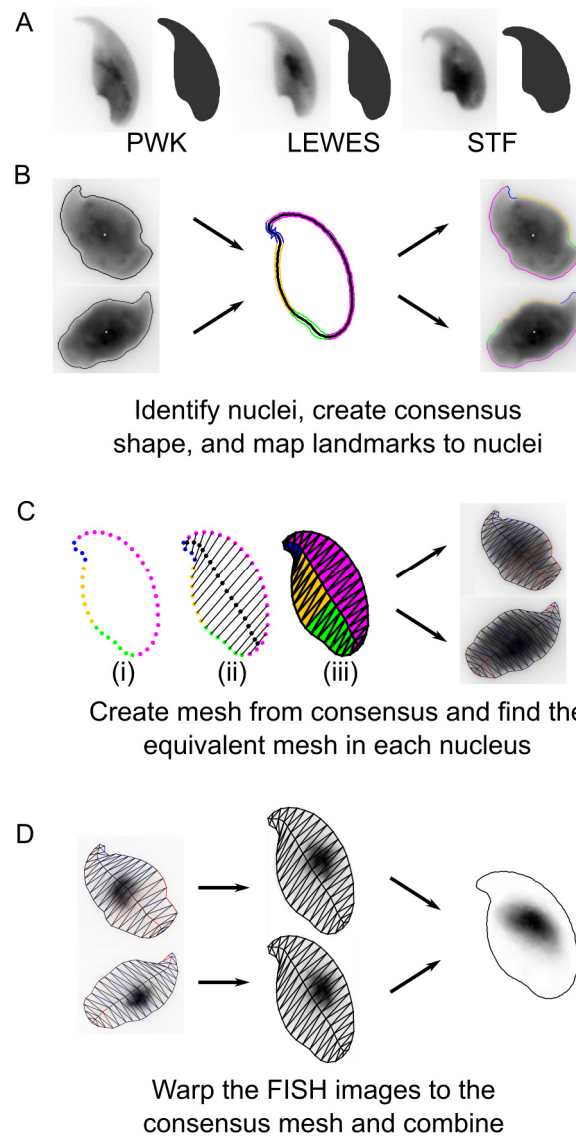
104

105 *2.3 Image analysis*

106

107 Analysis was performed using our image analysis software (Nuclear Morphology Analysis,
108 available from http://bitbucket.org/bmskinner/nuclear_morphology/wiki/Home/, version 1.15.0) for
109 morphometric analysis of mouse sperm shape [18]. Here, we combine nuclear morphometry with
110 FISH signal detection in order to rigorously quantify the distribution of chromosome territories within
111 the asymmetric mouse sperm head. Within our images we detected 1445 PWK nuclei, 906 LEWES
112 nuclei and 712 STF nuclei across all hybridisations (Figure 1B). The number of nuclei with FISH signals
113 detected which were used for chromosome positioning analysis are given in Supplementary Table 1.

114 This analysis, which we refer to as “nuclear cartography” is a form of mesh warping, achieved by
115 overlaying a mesh onto each individual sperm nucleus and quantifying the distribution of the
116 chromosomal signal within each face of the mesh (Figure 1C). This allows accurate, quantifiable 2D
117 analysis of the signal distribution in each cell. Subsequently, since the mesh overlaid onto each sperm
118 head is structurally equivalent, dynamic image warping is used to combine multiple individual
119 nuclear outlines onto the consensus shape of the cell population (Figure 1D). Using this method, signal
120 intensity can be averaged over multiple sperm heads, reducing the effect of background
121 inhomogeneities and revealing the consensus two-dimensional location of the signal in the population
122 as a whole.



123
 124
 125
 126
 127
 128
 129
 130
 131
 132
 133
 134
 135
 136
 137
 138
 139
 140
 141
 142
 143

Figure 1. The process of warping FISH images. A) Examples of un-FISHed nuclei from the three strains, as described in [18]. B) After FISH, nuclei are automatically identified and landmarks are discovered. C) A mesh is created from the consensus nuclear shape; (i) peripheral vertices are evenly spaced between landmarks; (ii) internal vertices divide vertex pairs from the tip; (iii) all vertices are joined. The equivalent mesh is constructed for each nucleus. D) The FISH signal image is transformed to move every pixel to its location in the consensus mesh. The warped images are combined to yield the composite signal image.

For successful warping of the source image, the face of the mesh to which each pixel belongs must be determined. The critical step is the construction of the mesh, such that each face contains a structurally equivalent region of the nucleus. First, we identify key landmarks around the periphery of the nucleus (i.e. the apical hook, tail attachment site, and other areas of maximal curvature), as described previously [18]. Next, semi-landmarks are constructed by spacing a set number of equidistant points between each landmark (Figure 1Ci). These then serve as the peripheral vertices of the mesh. The internal vertices are created by walking through the points pairwise from the tip of the nucleus, and generating a vertex at the centre of the line connecting each pair (Figure 1Cii). Internal and peripheral vertices are connected into the faces of the mesh (Figure 1Ciii). The same structural mesh is created for the consensus nucleus shape, and for each individual nucleus. An affine transform is applied to image pixels within each face, moving them to their equivalent positions in the consensus mesh. After pixels have been relocated, a gap-filling kernel sets any empty pixel to the average of the surrounding non-zero 8-connected pixels, as long as there are at least 4 non-zero surrounding pixels.

144 This reduces 'smearing' in cases where there is a large size difference between source and consensus
145 mesh faces.

146 In this way, we 'warp' the original images to fit the consensus nucleus. The warped images can be
147 combined to reveal the locations of consistent nuclear signal. Random noise is averaged out, while
148 consistent signals are reinforced. To avoid bias from higher or lower intensity signals in different
149 nuclei, the FISH images are binarised before warping. Since the individual images are being warped to
150 fit a template shape, it is possible to choose any template with the same underlying graph structure in
151 the mesh. This allows comparison of FISH signal distributions between different hybridisations.

152 To compare signal distributions between warped signals, we used an open source
153 implementation of a multi-scale structural similarity index measure, MS-SSIM* [19,20], which
154 quantifies visual similarity between images [21] on a scale of 0 (no similarity) to 1 (identical images).
155 To further assess adjacency of chromosome territories, we identified the chromosomal signals within
156 the nuclei by thresholding [3], and measured the distances between the centres of mass of
157 co-hybridised chromosomes. Statistical analyses were performed in R 3.5.1 [22], and charts were
158 generated using the cividis colour palette [23].

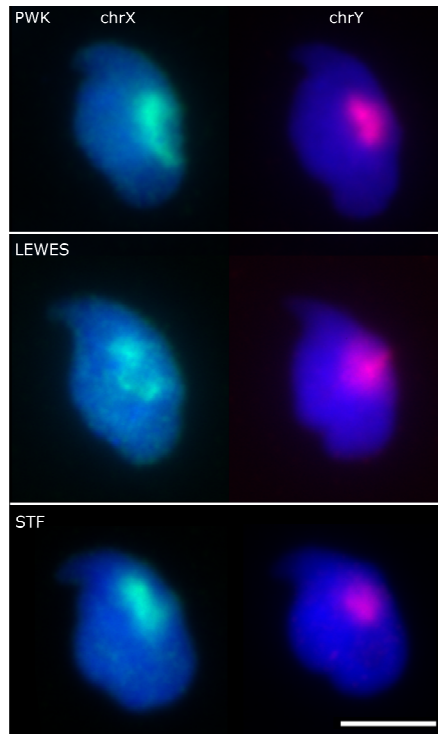
159 3. Results

160 3.1. *The sex chromosomes have conserved position in mouse sperm nuclei*

161 The process of hybridising FISH probes to sperm nuclei required a considerable swelling step
162 due to the highly compact chromatin. The nuclear area doubles from about $20\mu\text{m}^2$ to about $40\mu\text{m}^2$,
163 with the majority of the swelling in the dorsal/ventral axis (Figure S3). This swelling distorts the
164 nuclear shape; our method for automated nucleus and landmark detection [18] was able to identify
165 and orient swelled nuclei successfully, despite the fewer landmarks available.

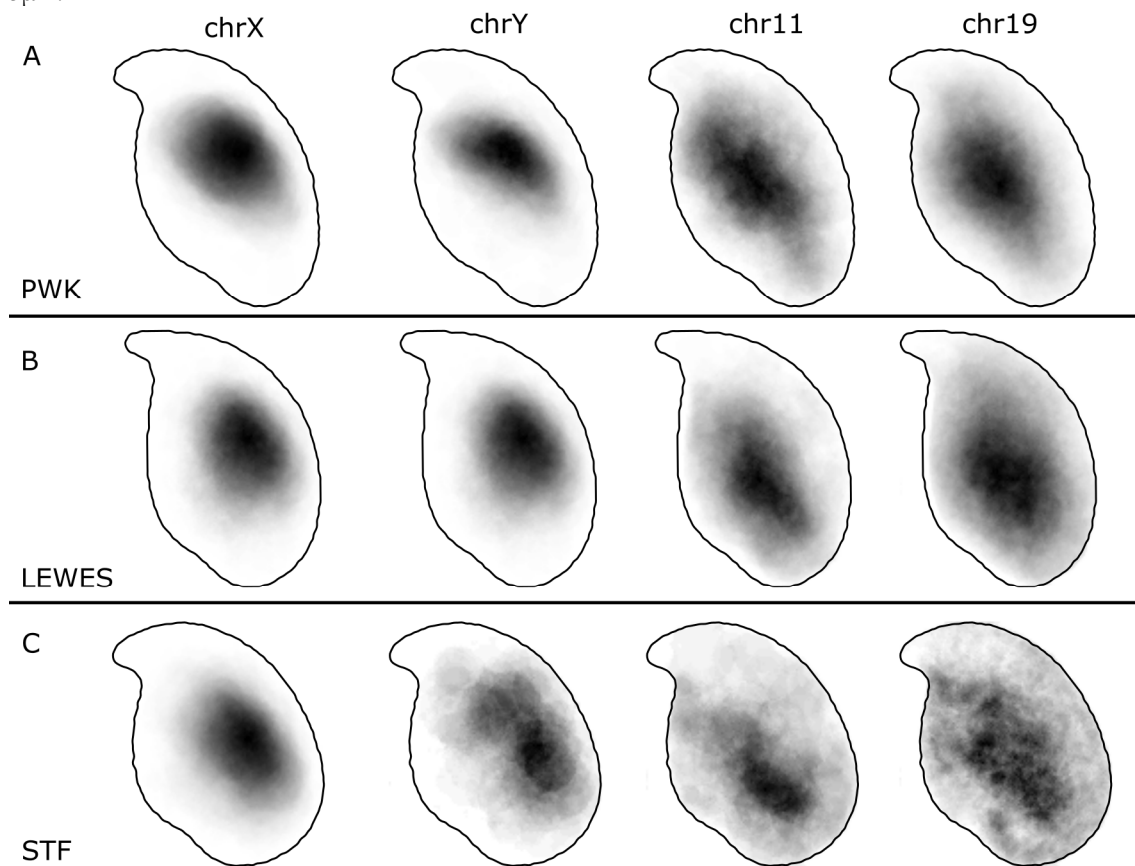
166 Confident that we could orient a FISH signal within the nucleus, we applied the new technique
167 to FISH images of mouse sperm from three strains, using chromosome paints for the X and Y
168 chromosomes. These have been previously reported in *M. musculus* strain C57Bl6 to lie under the
169 acrosome [8,9]. Nuclei and signals were detected from the captured images, a consensus nuclear
170 shape was calculated for each strain, and each FISH image was warped onto that consensus shape. A
171 composite image was created by layering each FISH image, providing - effectively - a heat-map of
172 signal location within the nucleus.

173 Our results confirm a consistent sub-acrosomal location for both X and Y chromosomes (Figure
174 2). Following the signal warping onto the population consensus, we observed that both X and Y
175 chromosomes have overlapping territories (Figure 3, 4).



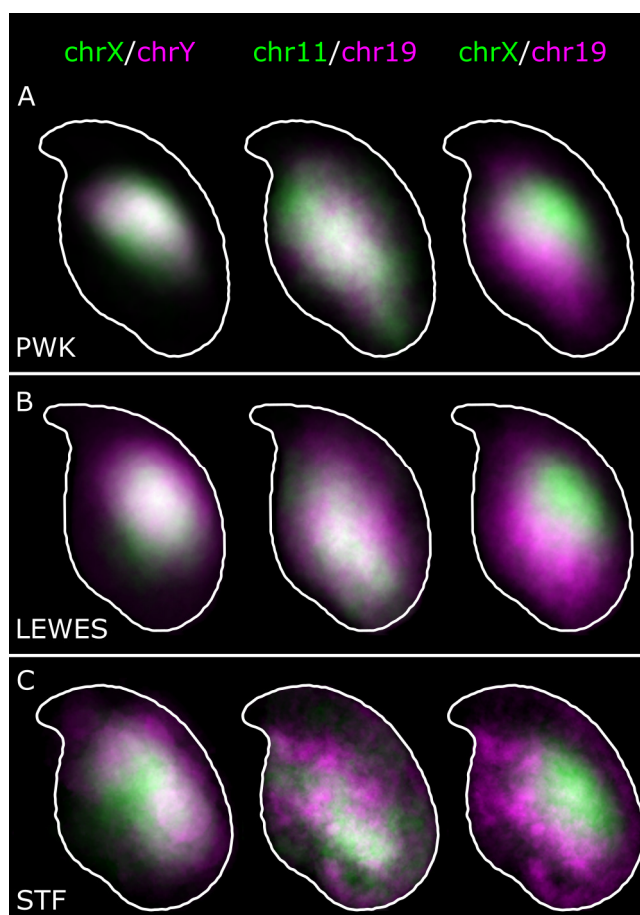
176
177
178
179

Figure 2. Example images showing the sex chromosome positions within the three strains. Scale bar represents 5 μ m.



180
181
182
183
184

Figure 3. Composite signal distributions for chromosomes X, Y, 11 and 19 in (A) PWK, (B) LEWES and (C) STF. The sex chromosomes occupy a consistent territory apical and dorsal to the centre of mass, generally under the acrosome but rarely extending fully to the periphery of the nucleus. Chromosomes 11 and 19 are more widely distributed, with the predominant location basal and ventral to the centre of mass.



185

186

187

188

Figure 4. Overlay of warped distributions from Figure 3 shows the similarities between chromosome X and Y territories, and 11 and 19 territories in (A) *M. m. musculus*; (B) *M. m. domesticus*; and (C) *M. spretus*. White shows regions of overlap. Chromosomes X and 19 (and X and 11) are predominantly non-overlapping.

189

190

3.2. Chromosomes 11 and 19 occupy similar nuclear addresses

191

192

193

194

195

196

197

With the sex chromosome locations confirmed to be conserved, we decided to examine two further chromosomes, both of which have previously been reported in the literature. Chromosome 19 has been described in C57Bl/6 mice to frequently lie toward the base of the nucleus [8]. Furthermore in Hi-C experiments, chromosomes X and 19 had a low association in *M. musculus* C57BL sperm chromatin; chromosome 19 and chromosome 11 had a moderate association with each other [17]. For this reason, we hypothesised that chr11 and chr19 might share a similar distribution, and that this would be distinct from that of the sex chromosomes.

198

199

200

201

202

203

204

205

206

207

The composite signal position data are shown in Figure 3. The patterns are indeed different to that of the sex chromosomes. The majority of the signal lies ventral and basal to the centre of the nucleus, yet there are clearly instances of signal throughout the nucleus, from the basal region near the tail attachment point to the apex and partially extending into the hook. Some examples of these positions in individual nuclei are shown in Figure 5. Although hybridization efficiency was poorer in *M. spretus*, the same patterns are apparent as in the *M. musculus* strains. Interestingly, we observed instances of both chr11 and chr19 below the acrosomal curve, in which the chr19 was generally more elongated than chr11 (see Figure 5B and F). Where chromosome 19 was co-hybridised with chromosome X, we were able to see rare instances of chrX and chr19 lying adjacent, with chrX more internal (Figure S1).

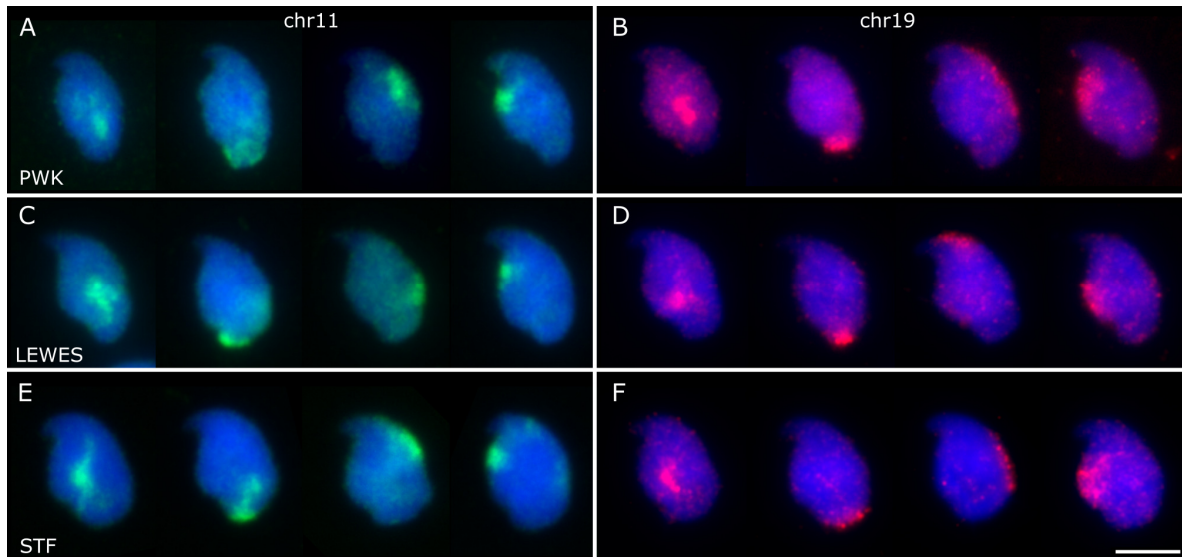
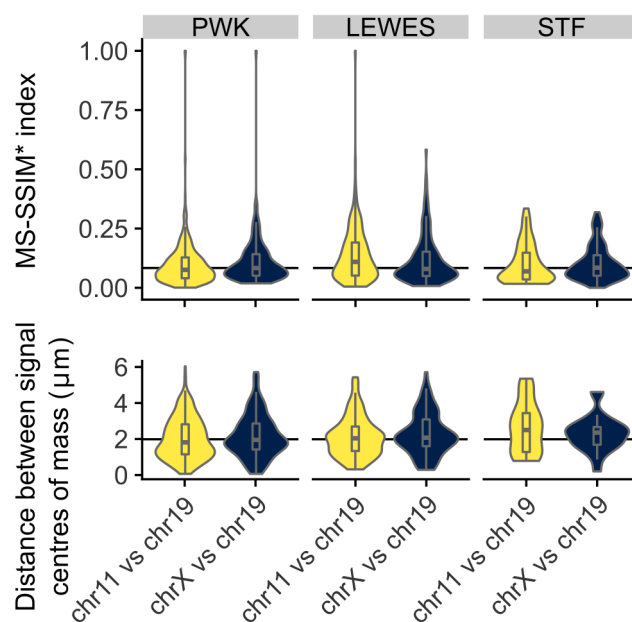


Figure 5. Examples of individual chromosome positions for chr11 (A, C, E) and chr19 (B, D, F) in the three strains; the chr11 and chr19 panels do not show the same nuclei. While the majority of the signals for each chromosome were observed ventral and basal of the nuclear centre (column 1), we found territories at the base of the nucleus (column 2), under the acrosome (column 3), and along the ventral surface below the hook (column 4). Scale bar represents 5 μ m.

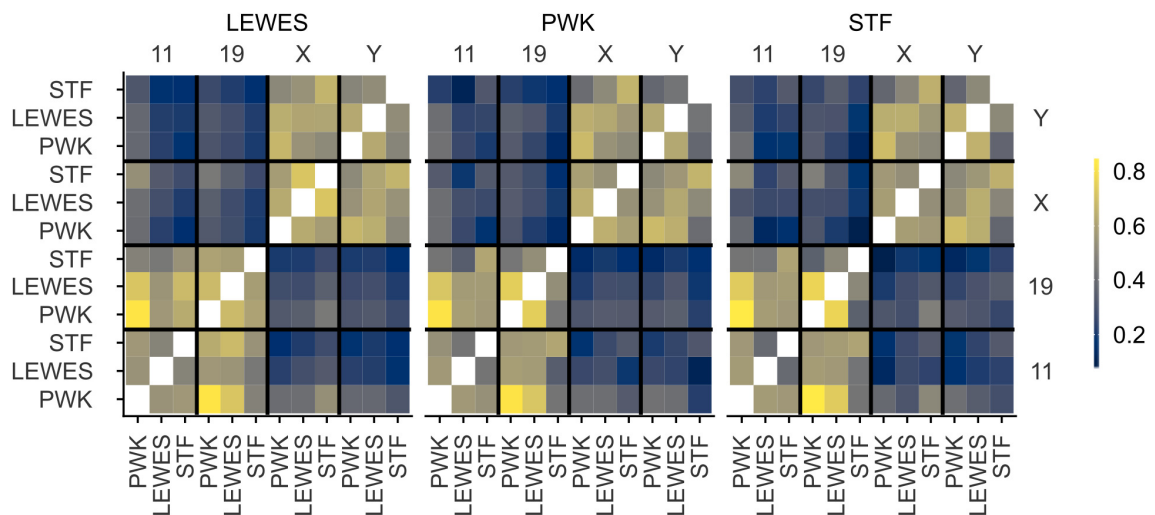
Given the similarity in overall signal distributions, we looked to see if chr11 and chr19 tend to lie adjacent to each other in individual nuclei. Visually, we can see that they are occasionally adjacent, but are not always associated. Measurement of the distance between the chromosome signal centers of mass showed no difference between chr11 and 19 or between chr11 and X, nor did a comparison of individual nucleus warped signal images via a multi-scale structural similarity index (MS-SSIM*), a technique also used in comparisons of radiological images [24] ($p > 0.05$, Wilcoxon rank sum tests; Figure 6). We conclude that, although chr11 and chr19 have a similar range of possible addresses to occupy within an individual sperm head, they do not necessarily interact, and are no more likely to be adjacent than chromosomes 11 and X. It is however important to appreciate that our data addresses chromosome territories as a whole, rather than individual loci, and further work will be needed to robustly compare our data with the Hi-C data from [17] (see also Discussion).



228 **Figure 6.** Chromosomes 11 and 19 do not colocalize within individual nuclei; colocalization of signals shows
 229 no difference comparing chr11 and chr19 as when comparing chrX and chr19 by either MS-SSIM* (upper) or the
 230 distances between the chromosome signal centers (lower).

231 3.3 Quantification of signal positions reveals conserved chromosome organisation across species

232 In order to quantify the similarity of signal locations both within and between strains, we
 233 warped images from all three strains onto the LEWES (domesticus) consensus outline. These
 234 consensus warped images were compared using MS-SSIM*, revealing the similarities in the range of
 235 possible nuclear addresses a chromosome could occupy in each strain. The X and Y territories had
 236 high structural similarity to each other in all three strains, and had high concordance between strains
 237 (Figure 7). Similarly, we saw greater similarity between chr11 and chr19 in all three strains. The
 238 pattern was slightly less clear between *M. spretus* and the other strains, presumably due to the lower
 239 hybridisation efficiency of the probes. To confirm there was no artefactual bias introduced by the
 240 choice of LEWES as the “destination” shape, we examined the effect of warping signals onto either
 241 the PWK or STF consensus outlines, and found that this made little difference in the values obtained
 242 (see also Figure S2, Table S2). This demonstrates that our method is robust for comparing differently
 243 shaped nuclei as long as we can define structurally equivalent landmarks.
 244



245 **Figure 7.** Similarity of signal distributions in composite warped images measured by MS-SSIM*, on a scale of
 246 0-1, where 0 indicates no similarity, and 1 indicates identical images. Images were warped in turn onto the
 247 consensus shapes of LEWES, PWK and STF. There is high correlation between the MS-SSIM* scores obtained
 248 when images are warped onto different target shapes (see Figure S2). Both within strains and between strains,
 249 there is a clear similarity between the distributions of chrX and chrY, and chr11 and chr19, but little similarity
 250 between the reciprocal combinations.
 251

252 4. Discussion

253 We have presented here a new method for quickly and efficiently mapping chromosome
 254 position in asymmetric nuclei, such as sperm, based on linking chromosome signals with
 255 morphometric information about nuclear structure. Using this analysis, we have been able to
 256 measure and quantify differences in chromosome territory position in sperm from three mouse
 257 strains. All mouse strains studied here diverged, at most, 3 million years ago [25,26], and the
 258 karyotypes of *M. musculus* and *M. spretus* both have 40 chromosomes [27]. *M. musculus* and *M.*
 259 *spretus* are able to produce hybrids in laboratory conditions, of which the female F1 is fertile [28]. We
 260 have demonstrated here that orthologous chromosomes adopt similar conformations in the three
 261 strains, despite differences in nuclear shape.
 262

263 4.1. Chromosomes X and Y have a conserved dorsal/sub-acrosomal position

264 Both the mouse X and Y chromosomes have been subject to massive amplification of
265 euchromatic sequences. The full sequence of a *M. m. musculus* C57Bl/6 Y chromosome revealed the
266 complex ampliconic structure [29], and demonstrated the presence of similar amplicons on the *M.*
267 *spretus* Y. These amplicons are thought to arise from genomic conflict in spermatids [30], and copy
268 number measurements of individual ampliconic genes suggests *M. spretus* has generally amplified
269 the same gene families as *M. musculus*, with the exception of X-linked H2a11, which has amplified
270 specifically in the *M. musculus* lineage.

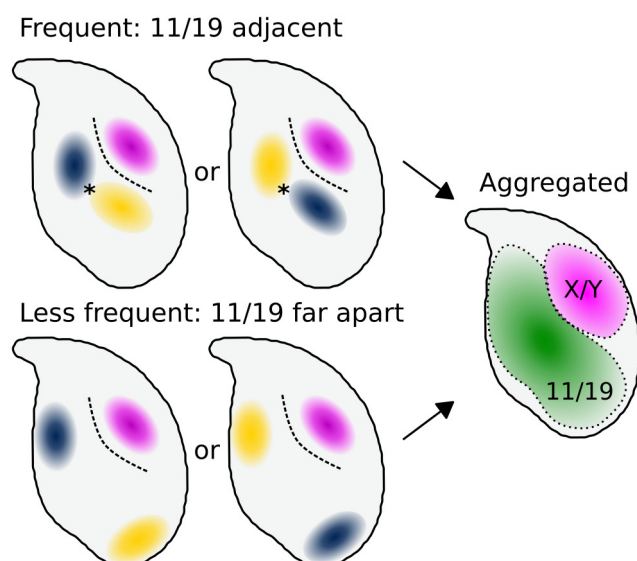
271 Despite the close evolutionary relationship of *M. musculus* and *M. spretus*, some small
272 rearrangements involving the sex chromosomes have been documented - for example, the *Clcn4*
273 gene, X-linked in most mammals including *M. spretus*, is autosomal in *M. musculus* [31], with clear
274 translocation breakpoints surrounding the gene [32].

275 Given the overall structural similarity of the orthologous chromosomes, it is likely they occupy
276 a similar volume within the nucleus, and are subject to similar conformational constraints. The sex
277 chromosomes have been previously described to adopt a dorsal position in the rodent sperm
278 nucleus [8,9], and have been seen to be sub-acrosomal in human, marsupial and monotreme sperm
279 [14]. It has been suggested that the X chromosome - in X-bearing sperm - is the first to enter the egg
280 during fertilisation. The position of the Y in marsupials is not reported, but as in mice, it is likely that
281 the Y adopts the same position as X simply because the space is available. In monotremes, the
282 platypus Y chromosomes do show a similar distribution to the X chromosomes [33]. Since the sex
283 chromosomes are different sizes - approximately 90Mb versus 170Mb - there must be differences in
284 the chromatin packing to allow them to occupy the same nuclear volume. In future we will be
285 interested to study the impact of chromosome constitution on nuclear morphology.

286 4.2 Chromosomes 11 and 19 have a conserved ventral/basal distribution

287 Chromosome 19 has been observed by others to lie in the basal region of the nucleus in
288 approximately two thirds of nuclei based on imaging and manually scoring at least 350 *M. musculus*
289 C57Bl/6 sperm nuclei [8,9]. Our results support these data, and demonstrate conservation of this
290 position across species. The signal in *M. spretus* is less clear, likely due to the cross-species
291 hybridisation, but the pattern is still distinguishable.

292 Our data from co-hybridisations suggest that although chr11 and chr19 adopt a similar overall
293 location, they do not always lie adjacent within a single nucleus. This indicates that while they have
294 preferred regions of the nucleus, they are mostly unconstrained with regard to each other.
295 Aggregate data from Hi-C experiments in C57Bl/6 sperm [17] have indicated that chr19 is
296 infrequently associated with the X chromosome (and by inference, the Y chromosome), and that
297 chr11 is only moderately associated with both chrX and chr19. It is however currently unclear why
298 Hi-C shows chromosome 19 to be more strongly associated with chromosome 11 than the X
299 chromosome, given our data showing that these three chromosome territories are on average
300 equidistant. One potential explanation is that while our measurements focus on the centre of each
301 chromosome territory, interactions occur at the periphery of territories in cells where they abut each
302 other. The mouse sperm head tends to have a DAPI-dense chromocenter “core”, and that the X/Y
303 and 11/19 regions are deduced to usually lie on opposite sides of this. Potentially this core forms a
304 barrier to inter-chromosomal interactions (Figure 8). As an analogy, Cersei and Jaime (chromosomes
305 11 and 19) may both live in the ground floor flat, but they do not take up the exact same physical
306 space, remaining on average a few meters apart. Meanwhile, their upstairs neighbor Daenerys
307 (chromosome X or Y) is roughly equidistant from them, but does not interact with them due to the
308 barrier in between (the centric heterochromatin). However, when averaged across the course of
309 many days, Cersei and Jaime collectively occupy the downstairs flat, while Daenerys occupies the
310 spatially distinct upper floor. A higher resolution investigation of individual loci found to be
311 associated in the Hi-C data will help resolve this distribution.
312



313
314 **Figure 8.** A simple model of how our data may relate individual cells to aggregate measurements. In
315 individual cells, chr11 and chr19 (blue/yellow) frequently lie adjacent, and more rarely further apart.
316 Chromosomes X and Y (purple) lie consistently below the acrosome. In contrast, chromosomes 11 and 19 do not
317 have strictly fixed addresses, but reside interchangeably within the same general area of the nucleus. Thus,
318 chromosomes 11 and 19 colocalise in the aggregate distribution despite not overlapping within any individual
319 nucleus. In this model, the chromocenter core acts as a physical barrier to interchromosomal interactions,
320 explaining why Hi-C detects more 11/19 interactions (indicated by *) than 11/X or 19/X interactions despite the
321 similar physical distances between the centres of mass of the three territories.
322

323 Overall, our measurements tend to support previous Hi-C and FISH findings in laboratory
324 mouse sperm, and provide evidence that the same patterns will be found in *M. spretus*. The concept
325 of ‘spatial synteny’ - the conserved 3D position of orthologous loci despite karyotypic
326 rearrangements - has been proposed [34], and there is increasing evidence for conserved nuclear
327 organization of genes following chromosomal rearrangements [35]. As we extend our studies, it will
328 be interesting to compare the positions of the full set of chromosomes, to better understand how the
329 shorter and fatter *M. spretus* nucleus maps on the longer, thinner *M. musculus* nucleus. Further
330 comparisons with other mouse strains with greater shape variability will also be of value; for
331 example BALB/c, which have frequent shape abnormalities and aneuploidies [18,36].

332 Studies of strains with other aneuploidies, chromosomal rearrangements or Robertsonian
333 fusions, which will additionally constrain chromosome territories will be of interest. In humans, no
334 gross morphological differences in sperm nuclei have been seen in men carrying Robertsonian
335 fusions [37]. However, in boars (*Sus scrofa*), while gross nuclear morphology was not perturbed in
336 animals carrying a t(13;17) Robertsonian translocation, differences were apparent in the positions of
337 the affected chromosomes [38]. Extending beyond mice, rats (*Rattus rattus*) have a much thinner
338 hooked sperm nucleus; rat chromosomes have been mapped in developing spermatids from stages
339 7-13. The nucleus is compressed from a structure which at stage 10 is markedly similar to a mature
340 mouse sperm nucleus [39]. The associated dynamics of nuclear reshaping during spermiogenesis,
341 and chromosome repositioning are an area of active research [10].

342 4.3 This method allows rapid screening of large numbers of nuclei

343 In this analysis, we examined more than 3000 nuclei, and the method scales to greater numbers
344 with little additional time or user effort after images have been captured. The warping algorithm
345 processed these nuclei in under half an hour on a desktop computer equipped with an Intel i5-2400
346 processor and 16Gb memory, with the total user time excluding image capture being a few hours.
347 This is of course experience and hardware dependent, but the key point is that the total analysis time
348 can be measured in hours rather than days. Importantly, our analysis does not rely on extensive
349 manual classification of chromosome position, making it less subjective than current approaches,

350 and amenable to automation. The use of a mesh to warp signals from different nuclei onto a single
351 template shape allows for quantitative measurements of the similarity of signal distributions
352 between images, and in principle will allow us to study small differences in locus position that have
353 been beyond the scope of current scoring systems. Beyond chromosome territory positioning, it is
354 also amenable to the study of single BAC probes, or any small probe generating a punctuate signal,
355 as long as sufficient nuclei are analyzed to generate an aggregate signal; together with Hi-C data this
356 will allow us to study which intra- and inter-chromosomal folding contacts are retained in the sperm
357 head, and address long standing questions of whether sperm chromatin organisation represents an
358 echo of round spermatid chromatin organisation, or prefigures future chromatin folding dynamics
359 in the fertilised zygote.

360 A further methodological interest would be to identify reliable internal structural features
361 within the nucleus, using DAPI or other stains. Currently we use only peripheral features as
362 landmarks, which puts limits on the accuracy of our mesh when deforming images. More internal
363 structural data would permit more complex morphometric approaches such as Teichmüller
364 mapping, which has been used successfully in analysis (for example) of wing shape in *Drosophila*
365 species [40].

366 5. Conclusions

367 Here we have demonstrated a new method for locating chromosome paints or other nuclear
368 signals within mouse sperm nuclei, which is in principle also applicable to other asymmetric nuclei,
369 including nuclei with fewer axes of asymmetry, such as spatulate sperm nuclei. We have used this
370 technique to confirm the non-random positioning of the sex chromosomes, and of chromosomes 11
371 and 19, and demonstrated quantitation of signal positions allowing comparison between different
372 strains and species. Importantly, we have integrated this method into existing open-source image
373 analysis software designed for other biologists.

374 **Supplementary Materials:** Figure S1: Chromosomes X and 19 co-hybridization; Figure S2: Comparison of
375 MS-SSIM* scores using different warping templates; Figure S3: Examples of swelled and unswelled nuclei;
376 Table S1: Numbers of nuclei analyzed, Table S2: Complete MS-SSIM* comparisons between warped composite
377 images.

378 **Author Contributions:** Conceptualization, BMS and PE; Methodology, BMS and PE; Software and Validation,
379 BMS; Investigation, JB, CCR; Data Curation and Formal Analysis, BMS; Visualization, BMS; Supervision and
380 Project Administration, PE; Writing - Original Draft, BMS and PE; Writing - Review and Editing, BMS, CCR,
381 JMG, ELL and PE; Resources, JMG, ELL, EEKK, NA and PE; Funding Acquisition, NA and PE.

382 **Funding:** BMS was supported by the Biotechnology and Biological Sciences Research Council (BBSRC,
383 BB/N000129/1). PE and CCR were supported by HEFCE (University of Kent) and by the BBSRC (BB/N000463/1).
384 JMG and ELL were supported by the Eunice Kennedy Shriver National Institute of Child Health and Human
385 Development of the National Institutes of Health (R01-HD073439 and R01-HD094787) and the National
386 Institute of General Medical Sciences (R01-GM098536). EEKK was supported by the National Science
387 Foundation Graduate Research Fellowship Program under Grant No. (DGE-1313190).

388 **Acknowledgments:** We thank the animal handling staff at the University of Montana.

389 **Conflicts of Interest:** The authors declare no conflict of interest. The funders had no role in the design of the
390 study; in the collection, analyses, or interpretation of data; in the writing of the manuscript, or in the decision to
391 publish the results.

392

393 References

- 394 1. Skinner, B.M.; Volker, M.; Ellis, M.; Griffin, D.K. An Appraisal of Nuclear Organisation in Interphase
395 Embryonic Fibroblasts of Chicken, Turkey and Duck. *Cytogenet Genome Res* **2009**, *126*, 156–164.
- 396 2. Foster, H.A.; Griffin, D.K.; Bridger, J.M. Interphase chromosome positioning in in vitro porcine cells and
397 ex vivo porcine tissues. *BMC Cell Biology* **2012**, *13*, 30.

- 398 3. O'Connor, R.E.; Kiazim, L.; Skinner, B.; Fonseka, G.; Joseph, S.; Jennings, R.; Larkin, D.M.; Griffin, D.K.
399 Patterns of microchromosome organization remain highly conserved throughout avian evolution.
400 *Chromosoma* **2018**.
- 401 4. Foster, H.A.; Abeydeera, L.R.; Griffin, D.K.; Bridger, J.M. Non-random chromosome positioning in
402 mammalian sperm nuclei, with migration of the sex chromosomes during late spermatogenesis. *J. Cell. Sci*
403 **2005**, *118*, 1811–20.
- 404 5. Millan, N.M.; Lau, P.; Hann, M.; Ioannou, D.; Hoffman, D.; Barrionuevo, M.; Maxson, W.; Ory, S.; Tempest,
405 H.G. Hierarchical radial and polar organisation of chromosomes in human sperm. *Chromosome Res.* **2012**,
406 *20*, 875–887.
- 407 6. Ioannou, D.; Millan, N.M.; Jordan, E.; Tempest, H.G. A new model of sperm nuclear architecture following
408 assessment of the organization of centromeres and telomeres in three-dimensions. *Sci Rep* **2017**, *7*.
- 409 7. Zalenskaya, I.A.; Zalensky, A.O. Non-random positioning of chromosomes in human sperm nuclei.
410 *Chromosome Res* **2004**, *12*, 163–173.
- 411 8. Kocer, A.; Henry-Berger, J.; Noblanc, A.; Champroux, A.; Pogorelnik, R.; Guiton, R.; Janny, L.;
412 Pons-Rejraji, H.; Saez, F.; Johnson, G.D.; et al. Oxidative DNA damage in mouse sperm chromosomes: Size
413 matters. *Free Radical Biology and Medicine* **2015**, *89*, 993–1002.
- 414 9. Champroux, A.; Damon-Soubeyrand, C.; Goubely, C.; Bravard, S.; Henry-Berger, J.; Guiton, R.; Saez, F.;
415 Drevet, J.; Kocer, A. Nuclear Integrity but Not Topology of Mouse Sperm Chromosome is Affected by
416 Oxidative DNA Damage. *Genes (Basel)* **2018**, *9*.
- 417 10. Namekawa, S.H.; Park, P.J.; Zhang, L.-F.; Shima, J.E.; McCarrey, J.R.; Griswold, M.D.; Lee, J.T. Postmeiotic
418 Sex Chromatin in the Male Germline of Mice. *Current Biology* **2006**, *16*, 660–667.
- 419 11. Finch, K.A.; Fonseka, K.G.L.; Abogrein, A.; Ioannou, D.; Handyside, A.H.; Thornhill, A.R.; Hickson, N.;
420 Griffin, D.K. Nuclear organization in human sperm: preliminary evidence for altered sex chromosome
421 centromere position in infertile males. *Hum. Reprod.* **2008**, *23*, 1263–1270.
- 422 12. Olszewska, M.; Wiland, E.; Kurpisz, M. Positioning of chromosome 15, 18, X and Y centromeres in sperm
423 cells of fertile individuals and infertile patients with increased level of aneuploidy. *Chromosome Res* **2008**,
424 *16*, 875–890.
- 425 13. Ioannou, D.; Griffin, D.K. Male Fertility, Chromosome Abnormalities, and Nuclear Organization.
426 *Cytogenet Genome Res* **2010**.
- 427 14. Greaves, I.K.; Rens, W.; Ferguson-Smith, M.A.; Griffin, D.; Marshall Graves, J.A. Conservation of
428 chromosome arrangement and position of the X in mammalian sperm suggests functional significance.
429 *Chromosome Res.* **2003**, *11*, 503–512.
- 430 15. Stevens, T.J.; Lando, D.; Basu, S.; Atkinson, L.P.; Cao, Y.; Lee, S.F.; Leeb, M.; Wohlfahrt, K.J.; Boucher, W.;
431 O'Shaughnessy-Kirwan, A.; et al. 3D structures of individual mammalian genomes studied by single-cell
432 Hi-C. *Nature* **2017**, *544*, 59.
- 433 16. Nagano, T.; Lubling, Y.; Stevens, T.J.; Schoenfelder, S.; Yaffe, E.; Dean, W.; Laue, E.D.; Tanay, A.; Fraser, P.
434 Single-cell Hi-C reveals cell-to-cell variability in chromosome structure. *Nature* **2013**, advance online
435 publication.
- 436 17. Battulin, N.; Fishman, V.S.; Mazur, A.M.; Pomaznoy, M.; Khabarova, A.A.; Afonnikov, D.A.;
437 Prokhortchouk, E.B.; Serov, O.L. Comparison of the three-dimensional organization of sperm and
438 fibroblast genomes using the Hi-C approach. *Genome Biology* **2015**, *16*, 77.

- 439 18. Skinner, B.M.; Rathje, C.C.; Bacon, J.; Johnson, E.E.P.; Larson, E.L.; Kopania, E.E.K.; Good, J.M.; Yousafzai,
440 G.; Affara, N.A.; Ellis, P.J.I. A high-throughput method for unbiased quantitation and categorisation of
441 nuclear morphology. *bioRxiv* **2018**, 312470.
- 442 19. Prieto, G.; Chevalier, M.; Guibelalde, E. MS_SSIM Index and MS_SSIM* Index as a Java plugin for ImageJ;
443 Department of Radiology, Faculty of Medicine. Universidad Complutense: Madrid. SPAIN., **2009**
- 444 20. Rouse, D.M.; Hemami, S.S. Analyzing the role of visual structure in the recognition of natural image
445 content with multi-scale SSIM. In *Proceedings of the Human Vision and Electronic Imaging XIII*;
446 International Society for Optics and Photonics, **2008**; Vol. 6806, p. 680615.
- 447 21. Wang, Z.; Bovik, A.C.; Sheikh, H.R.; Simoncelli, E.P. Image quality assessment: from error visibility to
448 structural similarity. *IEEE transactions on image processing* **2004**, *13*, 600–612.
- 449 22. R Core Team R: A Language and Environment for Statistical Computing; R Foundation for Statistical
450 Computing: Vienna, Austria, **2018**
- 451 23. Nuñez, J.R.; Anderton, C.R.; Renslow, R.S. Optimizing colormaps with consideration for color vision
452 deficiency to enable accurate interpretation of scientific data. *PLOS ONE* **2018**, *13*, e0199239.
- 453 24. Renieblas, G.P.; Nogués, A.T.; González, A.M.; Gómez-Leon, N.; del Castillo, E.G. Structural similarity
454 index family for image quality assessment in radiological images. *J Med Imaging (Bellingham)* **2017**, *4*.
- 455 25. Fabre, P.-H.; Hautier, L.; Dimitrov, D.; P Douzery, E.J. A glimpse on the pattern of rodent diversification: a
456 phylogenetic approach. *BMC Evol Biol* **2012**, *12*, 88.
- 457 26. Chevret, P.; Veyrunes, F.; Britton-Davidian, J. Molecular phylogeny of the genus *Mus* (Rodentia: Murinae)
458 based on mitochondrial and nuclear data. *Biol J Linn Soc* **2005**, *84*, 417–427.
- 459 27. Silver, L.M. *Mouse Genetics: Concepts and Applications*; Oxford University Press: Oxford, New York,
460 **1995**; ISBN 978-0-19-507554-0.
- 461 28. Palomo, L.J.; Justo, E.R.; Vargas, J.M. *Mus spretus* (Rodentia: Muridae). *Mamm Species* **2009**, 1–10.
- 462 29. Soh, Y.Q.S.; Alföldi, J.; Pyntikova, T.; Brown, L.G.; Graves, T.; Minx, P.J.; Fulton, R.S.; Kremitzki, C.;
463 Koutseva, N.; Mueller, J.L.; et al. Sequencing the Mouse Y Chromosome Reveals Convergent Gene
464 Acquisition and Amplification on Both Sex Chromosomes. *Cell* **2014**, *159*, 800–813.
- 465 30. Ellis, P.J.I.; Bacon, J.; Affara, N.A. Association of Sly with sex-linked gene amplification during mouse
466 evolution: a side effect of genomic conflict in spermatids? *Hum. Mol. Genet.* **2011**, *20*, 3010–3021.
- 467 31. Rugarli, E.I.; Adler, D.A.; Borsani, G.; Tsuchiya, K.; Franco, B.; Hauge, X.; Disteche, C.; Chapman, V.;
468 Ballabio, A. Different chromosomal localization of the *Cln4* gene in *Mus spretus* and C57BL/6J mice.
469 *Nature Genetics* **1995**, *10*, 466–471.
- 470 32. Nguyen, D.K.; Yang, F.; Kaul, R.; Alkan, C.; Antonellis, A.; Friery, K.F.; Zhu, B.; de Jong, P.J.; Disteche,
471 C.M. *Cln4-2* genomic structure differs between the X locus in *Mus spretus* and the autosomal locus in
472 *Mus musculus*: AT motif enrichment on the X. *Genome Res* **2011**, *21*, 402–409.
- 473 33. Tsend-Ayush, E.; Dodge, N.; Mohr, J.; Casey, A.; Himmelbauer, H.; Kremitzki, C.L.; Schatzkamer, K.;
474 Graves, T.; Warren, W.C.; Grützner, F. Higher-order genome organization in platypus and chicken sperm
475 and repositioning of sex chromosomes during mammalian evolution. *Chromosoma* **2009**, *118*, 53–69.
- 476 34. Veron, A.; Lemaitre, C.; Gautier, C.; Lacroix, V.; Sagot, M.-F. Close 3D proximity of evolutionary
477 breakpoints argues for the notion of spatial synteny. *BMC Genomics* **2011**, *12*, 303.

- 478 35. Dai, Z.; Xiong, Y.; Dai, X. Neighboring Genes Show Interchromosomal Colocalization after Their
479 Separation. *Mol Biol Evol* **2014**, *31*, 1166–1172.
- 480 36. Kishikawa, H.; Tateno, H.; Yanagimachi, R. Chromosome Analysis of BALB/c Mouse Spermatozoa with
481 Normal and Abnormal Head Morphology. *Biol Reprod* **1999**, *61*, 809–812.
- 482 37. Cassuto, N.G.; Le Foll, N.; Chantot-Bastaraud, S.; Balet, R.; Bouret, D.; Rouen, A.; Bhourri, R.; Hyon, C.;
483 Siffroi, J.P. Sperm fluorescence in situ hybridization study in nine men carrying a Robertsonian or a
484 reciprocal translocation: relationship between segregation modes and high-magnification sperm
485 morphology examination. *Fertility and Sterility* **2011**, *96*, 826–832.
- 486 38. Acloque, H.; Bonnet-Garnier, A.; Mompert, F.; Pinton, A.; Yerle-Bouissou, M. Sperm Nuclear Architecture
487 Is Locally Modified in Presence of a Robertsonian Translocation t(13;17). *PLoS One* **2013**, *8*.
- 488 39. Meyer-Ficca, M.; Muller-Navia, J.; Scherthan, H. Clustering of pericentromeres initiates in step 9 of
489 spermiogenesis of the rat (*Rattus norvegicus*) and contributes to a well defined genome architecture in the
490 sperm nucleus. *Journal of Cell Science* **1998**, *111*, 1363–1370.
- 491 40. Choi, G.P.T.; Mahadevan L. Planar morphometrics using Teichmüller maps. *Proceedings of the Royal
492 Society A: Mathematical, Physical and Engineering Sciences* **2018**, *474*, 20170905.